

Aero-Optic Effects in Turbulent Wall-Bounded and Free Shear Flows

Konstantin N. Volkov *

Abstract—Large-scale eddies and related aero-optic effects in a turbulent boundary layer, free mixing layer and free round jet are considered. The results obtained are used to analyze the distortions produced in the phase function of a coherent light beam by the turbulent fluctuations of the parameters of the medium. The results of numerical calculations are compared with the experimental data and computational data obtained from the solution of Reynolds-averaged Navier–Stokes equations. The results obtained can be beneficial for design and optimisation of systems based on coherent optical adaptive techniques.

Keywords: computational fluid dynamics, turbulence, large-eddy simulation, aero-optic

1 Introduction

A coherent beam propagating through a randomly inhomogeneous medium (e.g. turbulent boundary layer or shear flow) feels optical aberrations. While the periphery of the boundary layer produces relatively small aberrations of a regular character, processes in the inner region of the boundary layer determine the electromagnetic wave propagation.

Problems of coherent beam propagation through a substance have received a lot of consideration in the literature. However, most results are obtained for the propagation of laser beam in the turbulent atmosphere [1]. Almost in any part of the atmosphere, the major phase distortions are introduced by large-scale eddy structures (with the exception of the near-earth boundary layer, where optical distortions are determined by small-scale eddies). The influence of the atmospheric effects on coherent beam propagation is associated with relatively low frequencies and can well be revealed by contemporary experimental tools. The influence of turbulent mixing is due to fast (high-frequency) changes in the flowfield. Since the spatial scales and characteristic frequencies of turbulent flows may vary within several orders of magnitude, serious difficulties may be anticipated in direct measurements and numerical calculations [2, 3].

*School of Mechanical and Automotive Engineering, Faculty of Engineering, Kingston University, Friars Avenue, Roehampton Vale, SW15 3DW, London, United Kingdom, Email: k.volkov@kingston.ac.uk

The turbulent mixing causes refractive index fluctuations in space and time. A relation between the refractive index and the medium density can be taken on the basis of the Gladstone–Dale law [2, 4]

$$n(\mathbf{x}, t) = 1 + G(\lambda) \frac{\rho(\mathbf{x}, t)}{\rho_0},$$

where ρ_0 is a characteristic density (e.g. the density of an undisturbed medium). The Gladstone–Dale constant, G , depends on the wavelength of the propagating beam and the working fluid. Weak dependence on wavelength is ignored, and $G = 0.223 \times 10^{-3}$ for air.

As coherent beam propagates through a randomly inhomogeneous medium, its amplitude and phase are subjected to fluctuations corresponding to the structural changes (broadening, deflection, and splitting) of the beam, as shown in the Figure 1. The distortions produced in the amplitude characteristics of the beam are negligibly small as compared to fluctuations of the refractive index [2, 4].

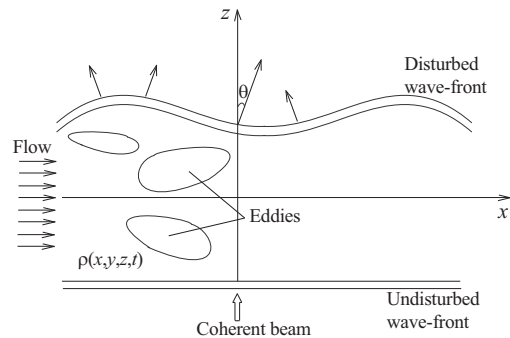


Figure 1. Propagation of coherent beam through a randomly inhomogeneous medium.

Because of the beam broadening, it cannot be focused at a large distance from the radiation source. As the diameter of the wave source grows, the diffraction spot at the focal point decreases to a certain finite radius (saturation size), rather than behaving as predicted in the optics of homogeneous media.

Fluctuations of the coherent beam's propagation direction shift the geometrical center of the beam in relation to the observation point.

The beam splitting shows up in a complex structure of

the light spot at a small distance from the wave source. At a large distance in the region of strong fluctuations, the coherent beam splits into thin threads with round or crescent-shaped cross sections. The optical energy is redistributed over the beam cross section, while the average power remains the same.

Scattering by random inhomogeneities of the medium also adds to the fluctuations of the intensity of electromagnetic radiation.

The effect of the refractive index fluctuations depends on the ratio D/L , where D is the beam diameter and L is the spatial period of the refractive index variations. At $D \ll L$, the refraction gradient is the same over the cross section of the beam and the beam deviates as a whole. At $D \sim L$, turbulence acts as a lens, which restructures the wave. At $D \gg L$, the turbulence deflects different elements in the cross section by different angles (light scattering).

In contrast to flows produced by turbulent mixing of medium (e.g. mixing layers and jets), atmospheric turbulent flows have a considerably large characteristic length and their losses for turbulent scattering are only insignificant [1].

2 Dispersion of phase fluctuations

Dispersion of small-scale fluctuations of density, σ_ρ^2 , and the corresponding correlation length scale, l_ρ , are related to the dispersion of wave phase, σ_φ^2 , by the expression

$$\sigma_\varphi^2 = \alpha\beta^2 \int_0^L \sigma_\rho^2 l_\rho dy, \quad \beta = \frac{2\pi}{\lambda} \frac{dn}{d\rho} = kG(\lambda), \quad (1)$$

where L is the optical path length, and the integral is taken across the boundary layer. The constant α depends on the form of the correlation function assumed for the density fluctuations (e.g. $\alpha = 2$ for the exponential correlation function and $\alpha = \pi$ for the Gaussian correlation function). According to the equation (1), this leads to an 11% difference in the dispersion of phase fluctuations.

Length scale l_ρ is found by integrating the correlation function

$$l_\rho = \int_{-\infty}^{+\infty} R_{\rho\rho}(y) dy.$$

In the conditions of local equilibrium, the correlation length scale coincides with the correlation scale of velocity fluctuations, $l_\rho \sim l_u \sim k^{3/2}/\varepsilon$. This assumption is not applicable near the wall, where velocity fluctuations turn to zero, therefore $k = 0$ and $l_u = 0$, but $l_\rho \neq 0$.

To estimate the phase fluctuations in the near-wall region, the formula (1) is usually replaced with a semi-empirical

formula [4]

$$\sigma_\varphi^2 = \beta^2 l_y \delta \sigma_\rho^2, \quad (2)$$

where l_y is the integral turbulence scale in the direction normal to the wall. It is assumed that $l_y \sim 0.1\delta$, where δ is the boundary layer thickness. The dispersion of the density fluctuations can be estimated as

$$\sigma_\rho^2 = A^2 (\rho_w - \rho_\infty)^2,$$

where ρ_w and ρ_∞ are the density at the wall and the density in the free flow, and $A = 0.1-0.2$. At $l_y \ll \delta$, formula (2) is refined by integrating across the boundary layer [4, 5]

$$\sigma_\varphi^2 = \beta^2 \int_0^L \sigma_\rho^2(y) l_y(y) dy. \quad (3)$$

Optical aberrations have been the subject of extensive experimental investigations, results of which are presented in [6–9].

LES of turbulent shear flows makes it possible to determine fluctuating parameters of a turbulent flow, including the field of density fluctuations [2, 10]. To this end, a number of semi-empirical models of different complexity have been elaborated. The most popular models are those described in [4] for homogeneous turbulence and in [11] for inhomogeneous turbulence. In models of [4, 5, 11] based on formulas (2) and (3), the dispersion of density fluctuations is determined as the difference between the density near the wall (inner region) and the density at the periphery region of the boundary layer (outer region). The applications of the models of [4, 11] are discussed in [5]. In the methods of [12, 13], the density fluctuations are found by solving the transport equation of a passive scalar.

If pressure fluctuations are disregarded, density fluctuations can be related to temperature fluctuations via the state equation [12, 13]. The temperature fluctuations are determined using the Reynolds analogy between the velocity and temperature fluctuations and the Prandtl mixing length model [14], whilst the accounting for the fact that the corresponding linear scales obey the relationship $l_u/l_T = Pr_t$, where the turbulent Prandtl number is taken to be constant.

Unlike solving the RANS equations, the use of DNS and LES makes it possible to obtain the field of density fluctuations, as well as the distributions of parameters σ_ρ^2 and l_ρ by solving the full (in DNS) or filtered (in LES) compressible Navier–Stokes equations [10].

A method for numerical simulation of the aero-optic characteristics of a subsonic air flow near a flat rectangular cave with regard to the field of turbulent fluctuations of the refractive index is proposed in [15]. The Reynolds

equations are closed using the Cockley model and the hypothesis of frozen stationary locally homogeneous and isotropic turbulence with the Kolmogorov spectrum. The optical characteristics of the turbulence are determined upon the local values of average aerodynamic fields. Fluctuations of pressure are neglected as compared to temperature fluctuations. However, in aerodynamic applications, this condition fails for the largest scale eddies [6], and the fluctuation parameters of the flow along with their average values are to be determined neglecting the microstructure of the turbulent flow.

In this study, the LES method is used to simulate aerodynamic effects in the boundary layer on a flat plate, in a free mixing layer, and in a round submerged jet. Large-eddy structures carrying maximal turbulent shear stresses and governed by the boundary conditions are found from the filtered Navier–Stokes equations. Small eddies have a universal structure and are simulated on the basis of a sub-grid scale (SGS) model. Unlike solving the RANS equations, the LES technique allows one to obtain the distributions of not only the average values but also the instantaneous quantities of a turbulent flow. The calculated data (field of the density fluctuations) are used to investigate the phase distortions induced in a coherent optical beam by the turbulent fluctuations of the flow parameters.

3 Phase function of wave front

The propagation of electromagnetic wave is described by Maxwell equations. Let us assume that the time scale related to the wave propagation is much smaller than the time scale of turbulence, refractive index is time-independent, and the medium is nonconducting and has a constant magnetic susceptibility. Then, the wave equation has the form

$$\nabla^2 \mathbf{E} - \frac{n^2}{c_0^2} \frac{\partial^2 \mathbf{E}}{\partial t^2} = 0, \quad (4)$$

where \mathbf{E} is the electric field strength. The refractive index is given by $n = c_0/c$, where c and c_0 are the velocities of light in the medium and free space, respectively. For a monochromatic sinusoidal wave with frequency ω , the equation (4) has an exact solution

$$\mathbf{E}(\mathbf{r}, t) = \mathbf{E}_0 \exp[\varphi(\mathbf{k}, \mathbf{r}) - \omega t], \quad (5)$$

where \mathbf{E} is the field strength at point \mathbf{r} at time moment t , and \mathbf{E}_0 is the field strength at the point $\mathbf{r} = 0$. The wave number, frequency, and wavelength are coupled by well-known relationships $k = \omega c = 2\pi/\lambda$.

The phase function of the wave front is given by

$$\varphi = \int \mathbf{k}(\mathbf{x}, t) \cdot d\mathbf{x},$$

where $\mathbf{k} = 2\pi\mathbf{l}/\lambda$ is the wave vector, and \mathbf{l} is a unit vector specifying the wave propagation direction.

When a plane monochromatic wave passes through a layer with a varying refractive index, its amplitude remains almost constant and the phase is changed, so that $\varphi = \varphi_0 + \Delta\varphi$, where $\Delta\varphi$ is the phase shift due to the inhomogeneity of the medium.

The field strength of a perturbed wave can be obtained by multiplying equation (5) by factor $\exp(i\Delta\varphi)$, where $\Delta\varphi(x, y)$ denotes the phase shift along the optical path length, $L = z_2 - z_1$. The phase distribution is found by integrating the distribution of the refractive index over the layer thickness

$$\Delta\varphi(x, y, t) = k \int_{z_1}^{z_2} \Delta n(x, y, z, t) dz,$$

where $\Delta n(x, y, z, t)$ is the variation of the refractive index along the propagation direction, z (across the flow).

In case the perturbations of the wave vector are small, the beam deflections can be neglected and the integral appears in the form

$$\varphi(x, y, t) = k_0 \int_{z_1}^{z_2} n(x, y, z, t) dz, \quad (6)$$

where $\varphi(x, y, t)$ is the phase distribution in plane (x, y) normal to the direction of wave propagation at time t .

The results of these calculations are usually represented in the form [6]

$$\tilde{\varphi}(x, y, t) = \frac{\varphi(x, y, t)}{k_0 L \Delta n} \simeq \frac{1}{L \Delta n} \int_{z_1}^{z_2} [n(x, y, z, t) - n_\infty] dz. \quad (7)$$

Along the direction of the beam propagation, from the equation (7) we have

$$\psi(x) = L \frac{\partial \tilde{\varphi}}{\partial x} = \frac{1}{\Delta n} \int_{z_1}^{z_2} \frac{\partial n}{\partial x} dz,$$

where L is the size of the region of turbulent mixing. The corresponding spectra follow the relationship

$$S_\psi(k_x L) \sim (k_x L)^2 S_\varphi(k_x L).$$

For the mixing layer, we assume that $\Delta n = |n_1 - n_2|$ and $L = 2\delta$, where δ is the local width of the shear region, and subscripts 1 and 2 refer to the flows involved in mixing. The values calculated for the jet are normalized to $\Delta n = |n_a - n_\infty|$ and $L = 2r_a$, where the subscripts a and ∞ refer to the parameters at the nozzle outlet and in submerged space.

4 Description of flow field

An unsteady flow of a viscous compressible gas is described by spatially filtered Navier–Stokes equations, which are complemented with the state equation of an ideal gas and a model of RNG sub-grid scale model [16]. The width of the filter is correlated with the step of the computational mesh.

Simulation of large-scale eddies requires unsteady boundary conditions to be set in compliance with the random character of the flow. Free shear flows are known to be unstable, and oscillations can be generated there even in the absence of external perturbation sources.

Let a velocity profile be specified at the nozzle section (at $|r| = r_a$) with random sinusoidal perturbations superposed

$$v_x(r, t) = \frac{u_a}{3} \left[1 + \tanh \left(\frac{0.5 - |r|}{2\delta} \right) \right] [1 + \alpha \sin(\text{Sh } t)],$$

where $\delta/r_a \sim 0.1$, $\text{Sh} = 0.45$, and $\alpha = 0.0025$. Small random perturbations are also imposed on the radial distribution of circumferential velocity

$$v_\theta(r, t) = 0.025 \exp[-3(1 - |r|)^2] \varphi,$$

where α is a random number from the interval $[0.5, 0.5]$. The radial velocity at the nozzle outlet is $v_r(r, t) = 0$.

Boundary conditions at a large distance from the jet flowing into the submerged space (at the lower and upper boundaries) depend on the ejection properties of the jet.

When mixing layer is simulated, velocity profile is specified at the input boundary of the calculation domain

$$u(y) = u_0 + \Delta u \tanh \left(\frac{y}{\delta} \right), \quad \delta = \frac{\Delta u}{(du/dy)_{y=0}}.$$

No-slip boundary conditions are specified on the walls, and non-reflecting boundary conditions are specified in the outlet section of the computational domain.

The filtered Navier–Stokes equations are discretized using the method of control volume based on and high resolution finite difference schemes [17]. For time discretization, the third-order Runge–Kutta method is employed. The flux is split into inviscid and viscous components. The inviscid fluxes are discretized by the method of piecewise-parabolic reconstruction (PPM) and the Chakravarthy–Osher scheme [18], and the viscous ones, by centered finite-difference formulas of the second order. The system of the difference equations is solved by the multigrid method.

5 Results and discussion

Calculations for the boundary layer on a flat plate are performed at a $180 \times 90 \times 90$ mesh. In this case, $x^+ = 45$,

$y_{\min}^+ = 1$ and $z^+ = 14$, where

$$y^+ = \left(\frac{u_\tau}{\nu_w} \right) y, \quad u_\tau = \left[\frac{\mu_w}{\rho_w} \left(\frac{\partial \langle u \rangle}{\partial y} \right)_w \right]^{1/2}.$$

Under these conditions, $\text{Re}_\delta = 2.6 \times 10^4$ (as calculated from boundary layer thickness, $\delta = 18$ mm) and $\text{Re}_{\delta_m} = 2.8 \times 10^3$ (as calculated from momentum thickness, $\delta_m = 2.2$ mm).

The resulting density fluctuations are by 10–20% higher than the experimental values, presented in [5] at $M = 0.88$ (see Figure 2). The maximum of the y axis distribution of the density fluctuations is located well close to the wall. At $0.2 < y/\delta < 0.6$, the root-mean-square density remains nearly constant and the dispersion of phase fluctuations is virtually uniform in this region.

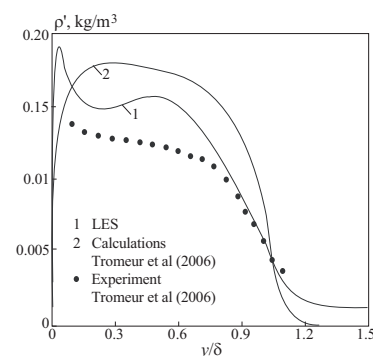


Figure 2. Density fluctuations in the boundary layer.

Comparison of the length scales l_u and l_ρ shows that they are equal only in the interval $0.1 < y/\delta < 0.22$. In the rest of the boundary layer, the correlation scale of the velocity fluctuations is considerably smaller than that of the density fluctuations.

The results of calculations concerning the boundary layer on a flat plate are shown in the Figure 3 (it is assumed that $\alpha = 2$). The plate has a constant temperature, $T_w = 300$ K. The dispersions obtained from formula (3) (line 4) are overestimated as compared to those calculated in accordance with model of [4] by formula (2) (lines 2 and 3). Unlike line 4, the dispersion of the wave phase provided by the LES calculations (line 1) has a kink point.

Following the Reynolds analogy, we assume that the correlation factor between the fluctuations of velocity and temperature is $R_{u'T'} = -1$. The results computed for large eddies indicate that, in the interval $0.12 < y/\delta < 0.86$, the correlation factor is nearly constant, $R_{u'T'} = -0.5$, which is in line with the data of [5].

Calculations for the mixing layer have been carried out for $\text{Re} = 2 \times 10^5$ (the Reynolds number is calculated from the momentum thickness) within the range $M_c = 0.15$ – 0.8 , where $M_c = (u_1 - u_2)/(a_1 + a_2)$, and a is the velocity of sound. At $M_c = 0.15$, compressibility has no effect on

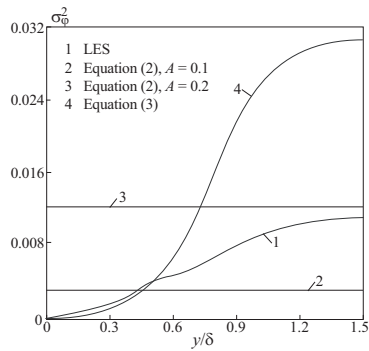


Figure 3. Dispersion of phase fluctuations in the boundary layer.

the properties of the flow ($\rho_2/\rho_1 = 1$), while at $M_c = 0.9$ the density ratio is $\rho_2/\rho_1 = 4$.

The profiles of the density fluctuations in the mixing layer are shown in the Figure 4 at $M_c = 0.8$. It is seen that the distributions of the density and pressure fluctuations in the cross sections of the mixing layer are similar with a maximum at the line separating the mixing flows. The profiles of pressure fluctuations are filled to a greater extent, and the maximal amplitude of the pressure fluctuations is close to a linear dependence on the streamwise coordinate. Small deviations from the linear dependence occur only at $x/L > 0.68$. The dependence of the maximal density fluctuations on the x coordinate is non-monotonic (see Figure 5). At $x/L < 0.6$, it is close to a linear one and, shows a peak and a smooth decay.

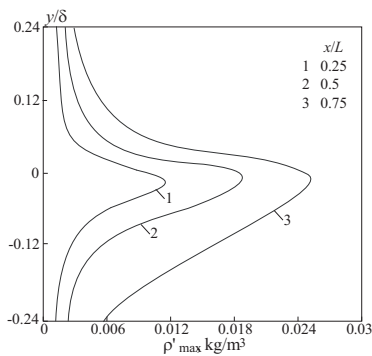


Figure 4. Density fluctuations in the cross section of the mixing layer.

In the intermediate range of wave numbers, the spectrum in the mixing layer shows the power dependence

$$S_\varphi(k_x L) \sim (k_x L)^{-q},$$

where $q \sim 2$ (see Figure 6). The compressibility only has a weak influence on the spectrum behavior (this influence is largely displayed at large wave numbers).

The density fluctuations grow with an increase in the effective Mach number. Calculations yields $l_\rho \sim 4l_u$, where $l_u = 0.2k^{3/2}/\varepsilon$.

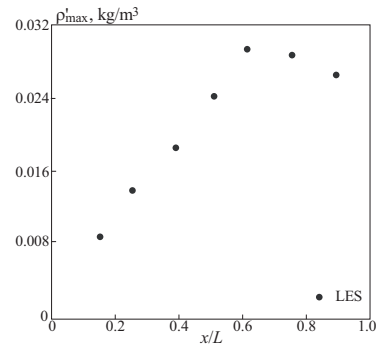


Figure 5. Dependence of the maximal density fluctuations in the mixing layer on streamwise coordinate.

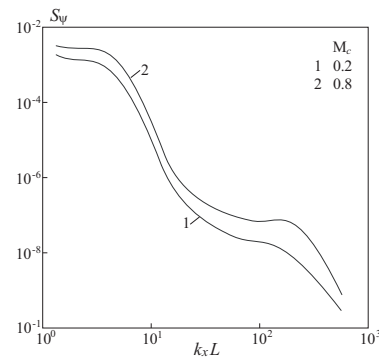


Figure 6. Spectrum of phase fluctuations in the free mixing layer.

Calculations of flow in the submerged round jet are carried out in the range $10^3 \leq Re \leq 10^5$ (Reynolds number is found from the velocity at the nozzle outlet and the nozzle diameter).

Large-scale eddy structures present in the shear layer and shown in the Figure 7 have the form of toroidal axially symmetric eddies nucleating certain distance apart from the nozzle outlet (of the order of one to two section diameters).



Figure 7. Contours of vorticity at time moment $t = 2.32$ s.

Eddy structures existing in the initial part of the jet are fairly small. The typical eddy size gradually increases from the start point downstream, thus, intensifying the exchange of momentum between the layer and the ambient fluid. The ellipsoidal shape of the coherent structure points to the anisotropy of turbulent pulsations in the region where large-scale eddies exist.

The generation of eddies is due to the Kelvin–Helmholtz instability of the shear layer. The maximum and minimum of the vorticity approximately correspond to the

eddy centers. At low Reynolds numbers, $Re \sim 10^3$, the jet at the nozzle outlet is nearly axially symmetrical. As the Reynolds number increases with distance from the nozzle (to $Re \sim 10^4$), a weak sinusoidal mode appears.

In the free jet at $Re = (2-8) \times 10^4$ and high wave numbers, $2r_a k_x > 1$, the wave spectrum is described by a

$$S_\varphi(k_x L) \sim (2r_a k_x)^{-q},$$

where $q \sim 2.5$ (see Figure 8). The spectrum for the jet is steeper than that for the mixing layer because of a stronger turbulent mixing, and is almost independent on the Reynolds number.

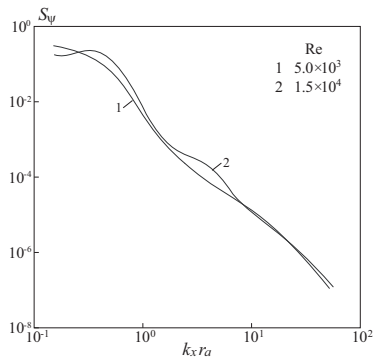


Figure 8. Spectrum of phase fluctuations in the round jet.

6 Conclusion

The large-eddy simulation of aero-optic effects in the boundary layer on a flat plate, in a free mixing layer, and in a round turbulent jet indicate that the spectrum of phase fluctuations is only a weak function of the input parameters (the dependence is stronger at large wave numbers). It is also shown that the use of semi-empiric models of turbulence leads to inaccurate values for the dispersion of phase fluctuations.

The results obtained may help to allow for density fluctuations in solving the RANS equations in the problem of optical wave propagation through a randomly inhomogeneous medium. The numerical procedures developed can be used to study the phase function distortions induced in a coherent beam by turbulent fluctuations of the medium parameters, as well as in optical measurement systems and some other devices.

The results obtained can be used for design and optimisation of systems based on coherent optical adaptive techniques (COAT).

References

1. Zuev V.E. *Propagation of visible and infrared radiation in the atmosphere*, New York, 1974.

2. Jumper E.J., Fitzgerald E.J., Recent advances in aero-optics, *Progress in Aerospace Sciences*, 2001, 37(3), pp. 299–339.
3. Gordeyev S., Jumper E.J. The optical environment of a cylindrical turret with a flat window and the impact of passive control devices, *AIAA Paper* 2005-4657.
4. Sutton G.W. Aero-optical foundations and applications, *AIAA Journal*, 1985, 23(10), pp. 1525–1537.
5. Tromeur E., Garnier E., Sagaut P. Analysis of the Sutton model for aero-optical properties of compressible boundary layers, *Journal of Fluids Engineering*, 2006, 128(2), pp. 239–246.
6. Dimotakis P.E., Catrakis H.J., Fourguette D.C. Flow structure and optical beam propagation in high-Reynolds-number gas-phase shear layers and jets, *Journal of Fluid Mechanics*, 2001, 433, pp. 105–134.
7. Wyckham C.M., Zaidi S.H., Miles R.B., Smits A.J. Characterization of optical wavefront distortions due to a boundary layer at hypersonic speeds, *AIAA Paper* 2003-4308.
8. Carroll B.F., Boulos E., Sytsma M., Cattafesta L.N., Hubner J.P., Sheplak M. Aero-optic measurement facility characterization, *AIAA Paper* 2004-0936.
9. Catrakis H.J., Aguirre R.C., Nathman J.C., Garcia P.J. Large-scale refractive turbulent interfaces and aero-optical interactions in high Reynolds number compressible separated shear layers, *Journal of Turbulence*, 2006, 7(54), pp. 1–21.
10. Volkov K.N., Emelyanov V.N. Aero-optic effects in turbulent flow and their simulation, *Technical Physics*, 2008, 53(2), pp. 217–223.
11. Sutton G.W. Effect of inhomogeneous turbulence on imaging through turbulent layers, *Applied Optics*, 1994, 33(18), pp. 3972–3976.
12. Truman C.R. The influence of turbulent structure on optical phase distortion through turbulent shear flow, *AIAA Paper* 92-2817.
13. Wei H., Chen C.P. A nonequilibrium algebraic model for turbulent density fluctuations, *International Journal of Heat and Mass Transfer*, 1996, 39(18), pp. 3989–3991.
14. Huang P.G., Coleman G.N., Bradshaw P. Compressible turbulent channel flows: DNS results and modeling, *Journal of Fluid Mechanics*, 1995, 305, pp. 185–218.
15. Koterov V.N., Savelev A.D., Tolstykh A.I. Numerical simulation of aero-optical fields near receiving harbour of air observatory, *Mathematical Simulation*, 1997, 9(1), pp. 27–39.
16. Yakhot A., Orszag S.A., Yakhot V., Israeli M. Renormalization group formulation of large-eddy simulation, *Journal of Scientific Computing*, 1986, 1, pp. 1–51.
17. Volkov K.N. Unstructured-grid finite-volume discretization of the Navier–Stokes equations based on high-resolution difference schemes, *Computational Mathematics and Mathematical Physics*, 2008, 48(7), pp. 1181–1202.
18. Chakravarthy S.R., Osher S. A new class of high-accuracy TVD schemes for hyperbolic conservation laws, *AIAA Paper* 85-0363.